Nuclear Materials and Energy 34 (2023) 101395

Contents lists available at ScienceDirect

Nuclear Materials and Energy

journal homepage: www.elsevier.com/locate/nme

Master curve testing of RPV steels using mini-C(T) specimens – Irradiation effects and censoring statistics

A. Das [a,b,*], P. Chekhonin [a], M. Houska [a], F. Obermeier [c], E. Altstadt [a]

[a] Helmholtz-Zentrum Dresden-Rossendorf, Bautzner Landstrasse 400, 01328 Dresden, Germany
[b] Chair of Radiochemistry/Radioecology, Technische Universität Dresden, 01062 Dresden, Germany
[c] Framatome GmbH, Paul-Gossen-Str. 100, 91052 Erlangen, Germany

ARTICLE INFO

Keywords:
Fracture mechanics testing
Sub-sized specimen
Reference temperature
Reactor pressure vessel steels
Master curve
Neutron-irradiation

ABSTRACT

Neutron irradiation-induced embrittlement of the reactor pressure vessel (RPV) leads to an increase in the reference temperature (T_0) of the RPV steel and reduces the operating lifetime of nuclear reactors. Fracture mechanics testing of RPV steels before and after neutron irradiation, which reveals the shift in T_0, is often limited by the shortage of irradiated material. To solve this, we tested sub-sized 0.16T C(T) specimens manufactured from already tested SE(B) standard Charpy-sized specimens using the Master Curve concept. The transferability of fracture mechanics data from 0.16T C(T) to standard Charpy-sized specimens forms an integral part of this study. To simplify the testing procedure, based on statistical data, we studied the impact of the slow stable crack growth censoring criterion of the ASTM E1921-21 standard on the determination of T_0. We also present a statistically based strategy for an optimized test temperature selection. We found that the results from the 0.16T C(T) specimens are comparable to the standard Charpy-sized specimens. RPV steels containing higher Cu and P contents exhibit a higher increase in T_0 after irradiation. We also found that the stable crack growth-censoring criterion did not influence T_0 significantly. Our results demonstrate the validity of 0.16T C(T) specimen testing and confirm the role of the impurity elements Cu and P in neutron embrittlement. We anticipate further research linking microstructure to the fracture properties of materials before and after neutron irradiation and the optimization of Master Curve testing using the results from our statistical analysis.

small samples

1. Introduction

Neutron irradiation-induced material embrittlement of the reactor pressure vessel (RPV) limits the continued safe operation lifetime of nuclear reactors. After neutron irradiation, the higher the increase in the reference temperature T_0, the temperature at which the median fracture toughness value is 100 MPa$\sqrt{m}$, the lower the irradiation resistance of a material. Fracture mechanics testing using the Master Curve concept determines the T_0 of materials and consequently the shift in T_0 after neutron irradiation. The Master Curve concept relates the median fracture toughness and the test temperature in the ductile to brittle regime taking into account the scatter in testing using a three-parameter Weibull distribution [1] and the specimen size effect [2]. The shape of the master curve tends to stay the same after neutron irradiation on various RPV steels [3], therefore, justifying the use of this concept. However, a common problem associated with Master Curve testing is the shortage of neutron-irradiated materials. Besides solving the material availability limitation [4], the miniaturization of test specimens also reduces the active sample volume.

The T_0 obtained from Charpy-sized three-point (single edge) bend specimens (SE(B)) of 10 × 10 × 55 mm dimension [5–8] was often smaller as compared to the T_0 obtained from 1T C(T) specimens [6,7,9] due to a loss of constraint. Nanstad et al. reported better compatibility of the T_0 obtained from 1T SE(B) as compared to 1T C(T) specimens [7]. The use of reconstituted samples and small specimen techniques [10,11] was beneficial for solving the limited material availability issue. Mini-C(T) or 0.16T C(T) specimens from RPV steels with 4 mm thickness [12–18] have previously reported similar T_0 values with similar locations of fracture initiation points as compared to larger C(T) specimens. Yamamoto and Miura [19] obtained similar T_0 values for mini-C(T) and 0.5T C(T) specimens while a difference of 12–14 K between mini-C(T) and large C(T) specimens was reported by others [9,20]. Chaouadi et al. reported a bias of ±10 K between standard Charpy-sized and mini-C(T) specimens [9]. Sub-sized SE(B) samples with 3.33 mm

"Small samples" (Thermal aging (2/2) -no3)

* Corresponding author at: Helmholtz-Zentrum Dresden-Rossendorf, Bautzner Landstrasse 400, 01328 Dresden, Germany.
E-mail address: a.das@hzdr.de (A. Das).

https://doi.org/10.1016/j.nme.2023.101395
Received 20 May 2022; Received in revised form 21 November 2022; Accepted 20 February 2023
Available online 21 February 2023

thickness provided lower T_0 values as compared to mini-C(T) specimens by about 12.5 K [13]. It is clear that the comparison of T_0 obtained from small and larger specimens is not straightforward and needs further validation. Therefore, we tested 0.16T mini-C(T) specimens manufactured from already tested SE(B) standard Charpy-sized specimens using the Master Curve concept and obtained the reference temperature T_0 for RPV steels (in unirradiated and irradiated states). We then compared the reference temperatures of the mini-C(T) specimens with the standard Charpy-sized specimens.

Impurities like Cu and P in RPV steels induce neutron embrittlement due to the formation of Cu-rich [21,22] and phosphide precipitates [21,23] and can lead to an increase in T_0 [24]. To investigate the effect of the chemical composition on neutron irradiation, we chose two western RPV steels in this study, JRQ, and JFL. JRQ was used as an International Atomic Energy Agency (IAEA) reference material in the 1980s [25] and contains higher amounts of Cu and P that results in embrittlement during neutron irradiation. JFL, on the other hand, is an RPV steel that is similar to 22NiMoCr3-7 and found its use in German nuclear power plants [26]. Due to the manufacturing process and purity of JFL (lower Cu and P content), we expect it to be more resistant to neutron irradiation.

The selection of testing temperature in Master Curve testing of small-scale specimen is delicate as testing temperatures close to T_0 may lead to censoring due to the fracture toughness K_{Jc} exceeding the $K_{Jclimit}$ and/or violating the $K_{Jc\Delta a}$ criteria (slow stable crack growth before cleavage) of ASTM E1921-21 [27]. On the other hand, testing at too low temperatures ($T-T_0 < -50$ K) also leads to test results being invalid. While censoring of data in large sample pools is generally not a big problem, censoring in smaller pools (for example in neutron-irradiated specimens) can be a cause of concern as the validity criterion of ASTM E1921 $\sum r_i \cdot n_i \geq 1$ might not be fulfilled (where r is the number of uncensored valid data and n is the specimen weighting factor, which depends on the $T-T_0$ value). It was reported in [13] that a $T-T_0$ value below -30 K prevented the censoring of tests. In this study, based on the Master Curve testing results of a large number of mini-C(T)s from different RPV steels we develop a strategy to optimize the determination of the next test temperature to fulfill the validity criterion of $\sum r_i \cdot n_i \geq 1$. Two competing aspects must be taken into account:

- Testing at comparatively high temperatures close to T_0 to improve the quality of the fit (and obtain the highest weighting factor n)
- Avoiding censoring: this speaks for testing at comparatively low temperatures but not below $T-T_0 = -50$ K

While the $K_{Jclimit}$ censoring criterion can be checked easily during the Master Curve analysis, the $K_{Jc\Delta a}$ censoring criterion requires an additional optical or scanning electron microscope (SEM) investigation of the fracture surface. In this study, we check the effect of the violation of the $K_{Jc\Delta a}$ criterion (section 8.9.2 and 10.2.1 of ASTM E1921-21) on the determination of T_0 to simplify the Master Curve analysis procedure.

There are four objectives in this study:

1. To determine the shift in T_0 of JRQ and JFL from the unirradiated to the irradiated state and to study the effect of neutron irradiation on materials with different chemical compositions.
2. To validate the use of mini-C(T) specimens by comparing their T_0 values to standard Charpy-sized specimens.
3. To optimize the determination of the testing temperature within a sample ensemble using a probability function based on a large number of tests.
4. To study the impact of the stable crack growth censoring criterion ($K_{Jc\Delta a}$) on the determination of T_0.

2. Materials and methods

2.1. Materials

We focussed on two RPV steels in this work, the first is a base metal, ASTM A508 class 3, which is the IAEA reference material 1JFL11. We refer to this material as JFL in this work. Kawasaki Steel Corporation manufactured JFL through casting, forging and heat-treatment, which included austenization at 880 °C with oil quenching followed by tempering at 640 °C for 9 h with air-cooling. The second material is also a base metal, ASTM A533B class 1, which is the European reference material 3JRQ57. We refer to this material as JRQ in this work. The manufacturing of JRQ involved casting and rolling. Heat-treatment that followed included austenization at 900 °C with oil quenching, tempering at 665 °C for 12 h and stress release annealing at 620 °C for 40 h. Further details about the material can be found in [28]. The composition of both the materials is listed in Table 1. The composition of JRQ is very similar to that of JFL except that it contains higher amounts of Cu and P.

Based on a large number of tests, the censoring statistics of mini-C(T) specimens are compiled. The database includes a total number of 381 mini-CT tests from 11 different materials. The chemical compositions are listed in Table 1.Table 2 contains the mechanical properties (yield strength at room temperature (RT), Charpy impact transition temperature at 41 J and the upper shelf energy from Charpy impact tests) along with the total number N of valid tests carried out (uncensored + censored data). A combination of base and weld metals both in their unirradiated (300 samples) and irradiated states (81 samples) are included in the statistics. With a few exceptions, most of the materials also contributed to the verification of the $K_{Jc\Delta a}$ censoring criterion. For this, the measurement of the ductile crack growth region was performed according to ASTM E1921 using either an optical or a scanning electron microscope. The use of SEM was found to be more suitable for ductile crack growths that were close to the limit of $K_{Jc\Delta a}$ censoring criterion.

2.2. Irradiation conditions

Samples of JFL and JRQ were neutron-irradiated in the WWER-2 reactors in Rheinsberg up to a fluence of 10^{20} n/cm^2 at 255 °C [5]. This fluence correspond to approximately ten times the German end-of-life (EOL) criterion, which limits the maximum neutron fluence in RPV walls of pressurised water reactors to 10^{19}n/cm^2 (E > 1 MeV) [36]. Table 3 lists the irradiation details.

2.3. Master Curve testing

Master Curve testing was performed on unirradiated and neutron irradiated 0.16T mini-C(T) specimens of JFL and JRQ. The number of samples tested for each state can be found in Table 2. Typically, eight 0.16T C(T) samples were extracted from one standard Charpy SE(B) specimen, four from each half as shown in Fig. 1 which shows an example of a L-T oriented SE(B) specimen half used to manufacture four L-T oriented 0.16T C(T) specimen. The determination of reference temperature T_0 was performed using the multi-temperature method according to ASTM E1921-21 [27]. 0.16T C(T) specimens were tested with fatigue pre-cracking and 20% side grooving in the unirradiated state while the specimens were not side grooved in the irradiated state. It was reported that side grooving neither significantly affected the determination of T_0 [9,19] nor the location of the fracture initiation [18].

The specimens were monotonically loaded with a test speed of 0.1 mm/min quasi-statically using the Inspekt10 machine (10 kN maximum force) for the unirradiated specimens and using the MTS 50 machine (50 kN maximum force) fitted with a 10 kN load cell to increase precision for the irradiated specimen. The irradiated specimens were tested in the hot cells of Helmholtz-Zentrum Dresden-Rossendorf (HZDR). Sandner clip-on gauges were used on the front face to measure the front face

Table 1
Composition of all materials included in this study.

Common name	Material	C	Si	Mn	Cr	Ni	Mo	Cu	P	V
				Base Metals						
3JRQ57/5JRQ56B1	A533B Cl.1 [25]	0.18	0.24	1.42	0.12	0.84	0.51	0.14	0.017	0.002
1JFL11	A508 Cl.3 [26]	0.17	0.25	1.42	0.16	0.75	0.52	0.01	0.002	0.004
ANP-3	22NiMoCr3-7 [29]	0.23	0.20	0.70	0.44	0.98	0.79	0.12	0.015	–
Biblis-C	22NiMoCr3-7 [30]	0.21	0.2	0.90	0.41	0.87	0.53	0.04	0.008	0.007
GW8-BM /FZD-4	15Kh2MFAA [31]	0.15	0.30	0.45	2.86	0.10	0.79	0.05	0.008	0.31
CRIEPI	SQV2A [17]	0.22	0.25	1.46	0.11	0.69	0.57	–	0.002	–
				Weld Metals						
ANP-6	S3NiMo1 [29]	0.05	0.15	1.41	0.07	1.69	0.46	0.08	0.012	0.004
ANP-2	S3NiMo1 [31]	0.06	0.08	1.05	0.04	1.02	0.63	0.03	0.017	<0.01
ANP-5	NiCrMo1 [32]	0.08	0.15	1.10	0.74	1.11	0.60	0.22	0.015	0.001

Table 2
Materials included in censoring statistics with their irradiation state, mechanical properties, total number of specimens tested (N) and whether they are included in the verification of the $K_{Jc\Delta a}$ censoring criterion.

Common name	Material	Condition	Yield Strength at RT (MPa)	T41J Charpy (°C)	Upper shelf energy (J)	N	$K_{Jc\Delta a}$
3JRQ57	A533B Cl.1	Unirradiated[5,26]	484	−13.2	192.3	28	Yes
		Irradiated[5,26]	843	208.5	111.4	14	Yes
5JRQ56B1		Unirradiated	484	−13.2	192.3	25	No
CRIEPI	SQV2A (A533B Cl.1)	Unirradiated[17]	477.4	−90	–	39	Yes
1JFL11	A508 Cl.3	Unirradiated[26]	470	−42.6	211.2	41	Yes
		Irradiated[5,26]	640	35.7	195.5	36	Yes
ANP-3	22NiMoCr3-7	Unirradiated[6,32,33]	516	−50	194	16	Yes
		Irradiated[32]	530	–	–	16	Yes
Biblis-C		Unirradiated[34]	444	−42	186	17	No
GW8-BM	15Kh2MFAA	Unirradiated	534	–	–	20	No
FZD-4		Unirradiated[31]	531.8	−55	191	34	Yes
ANP-6	S3NiMo1	Unirradiated[32,35]	555	−55	174	31	Yes
		Irradiated[32,35]	817	123	–	15	Yes
ANP-2		Unirradiated[32,35]	516	−7	197	18	Yes
ANP-5	NiCrMo1	Unirradiated[32,35]	604	−12	145	31	Yes

Table 3
Neutron irradiation conditions for tested specimens.

Common name	Material	Fluence (10^{19}n/cm^2 E > 1 MeV)	Max flux (10^{12}n/cm^2/s E > 1 MeV)	Irradiation Temperature (°C)	Irradiation time (Days)
3JRQ57	A533B Cl.1	9.82	5.37	255	297
1JFL11	A508 Cl.3	8.67	4.74	255	297

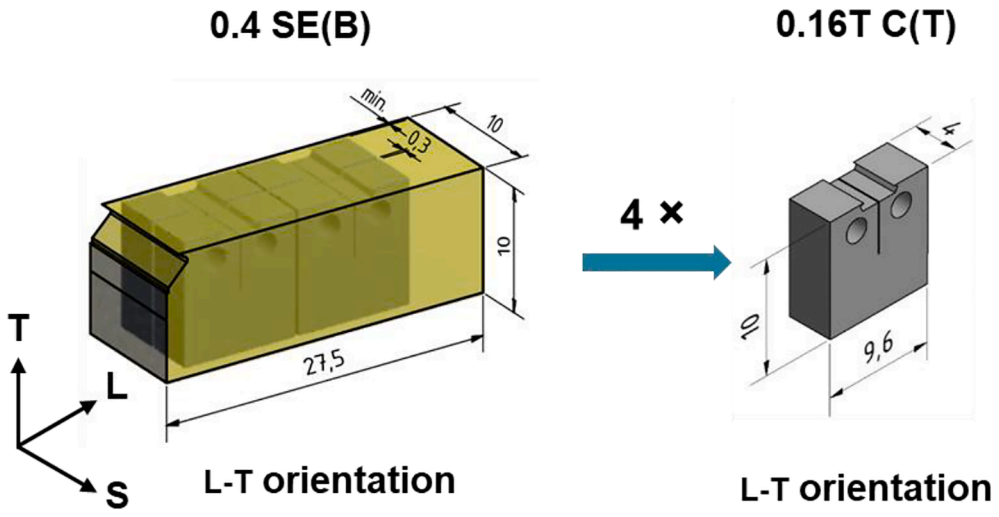

Fig. 1. Cutting scheme of 0.16T C(T) specimens manufactured from a standard Charpy SE(B) specimen.

displacements (FFD) which are converted to load-line displacements (LLD) using the conversion method as stated by Landes [37] with a rotation factor of $R = 0.352$.

A preliminary T_0 for the 0.16T C(T) specimen was assumed to be 20 K lower than the reference temperature determined for pre-cracked standard Charpy-sized specimens using the Master Curve concept [17]. Guided by the statistically based concept for optimum test temperature selection (discussed later in sections 3.3 and 4.3), the tests were performed at temperatures below the reference temperature of the mini-C(T) specimens until failure (most often by cleavage fracture). The initial crack lengths were measured at nine equally spaced points as required in ASTM E1921-21 using optical microscopy. The recorded load-displacement values were used to calculate the K_{Jc} values for the individual tests, which were thereafter used to plot the master curves. To check the violation of the $K_{Jc\Delta a}$ censoring criterion, an additional optical or scanning electron microscope investigation of the fracture surface was performed and the slow stable crack growth at the longest crack dimension was measured as mentioned in ASTM E1921-21.

3. Results

3.1. Irradiation-induced shift in reference temperature

K_{Jc} values obtained from fracture toughness testing are converted to K_{Jc} 1T equivalent values and are plotted (as open circles) against testing temperature in Figs. 2-4. The values marked as crosses are invalid values either due to failing the $T - T_0 > -50\,^{\circ}C$ invalidation criterion or due to an invalid crack shape [27]. The values marked as triangles are fracture toughness values which exceed the $K_{Jclimit}$ and/or the $K_{Jc\Delta a}$ censoring criterion. These values are censored during the determination of T_0 i.e. replaced either by the $K_{Jclimit}$ value or the highest uncensored K_{Jc} value depending on which criterion is violated. The reference temperature T_0, defined as the temperature when K_{Jc} median reaches a value of 100 MPa$\sqrt{m}$, is determined using ASTM E1921-21.

The K_{Jc} median (dashed) along with the 98% and 2% tolerance bound curves for the unirradiated and irradiated states for JRQ in the T-L orientation and JFL in the L-T and T-S orientation are shown in Fig. 2, Fig. 3 and Fig. 4, respectively. The dotted validity window is drawn with the temperature limits of $T_0 \pm 50K$ and the $K_{Jclimit}$ values are calculated using the lowest ligament length of the test series. On the other hand, the individual $K_{Jclimit}$ values in the Master Curve analysis were calculated using varying ligament lengths. Therefore, in some instances (like in Fig. 2 JRQ irradiated), a valid data point may appear outside the validity window, but in reality, it is not. The reference temperature (T_0) and the shift in reference temperature (ΔT_0) along with the number of valid uncensored tests (r), total number of valid tests (N), the value of $\sum r_i \cdot n_i$ and the standard deviation (σ) from both the unirradiated to the irradiated states are listed in Table 4. The highest value of $\sum r_i \cdot n_i$ was obtained for the unirradiated testing of JFL in the T-S orientation and lowest was obtained for the unirradiated testing of JRQ in the T–L orientation. Testing in different orientations T-L, T-S and L-T resulted in reference temperatures which varied less than or equal to the standard deviation of the test series.

An increase in the reference temperature was observed for both materials from unirradiated to the irradiated state, more for JRQ as compared to JFL (Fig. 5 and Table 4). For the JFL material, a change in the orientation resulted in only a small difference in the shift in reference temperature (ΔT_0).

3.2. Comparison of standard Charpy-sized and mini-C(T) specimen

The results of MC testing for the standard Charpy-sized specimens can be found in reference [5]. In Table 5, the reference temperatures and standard deviations determined from the standard Charpy SE(B) specimens and the 0.16T C(T) specimens are listed along with $\Delta\theta$ (the difference between the reference temperatures of standard Charpy-sized and mini-C(T) specimens) for JRQ and JFL. These two materials were selected for size comparison since in our study the mini-C(T)s were directly manufactured from the standard Charpy-sized specimens and exposed to the same irradiation conditions facilitating a direct comparison. This was not possible for other materials in Table 1. The reference temperatures of both materials in the unirradiated and the irradiated states is given in Fig. 6 and Fig. 7, respectively. Standard deviations are given as error bars. The reference temperatures of the 0.16T C(T) specimens lie within the error bars of the standard Charpy SE (B) specimens for all the unirradiated and irradiated cases except for the unirradiated T-S orientation of JFL (if compared with Charpy SE(B) L-T samples).

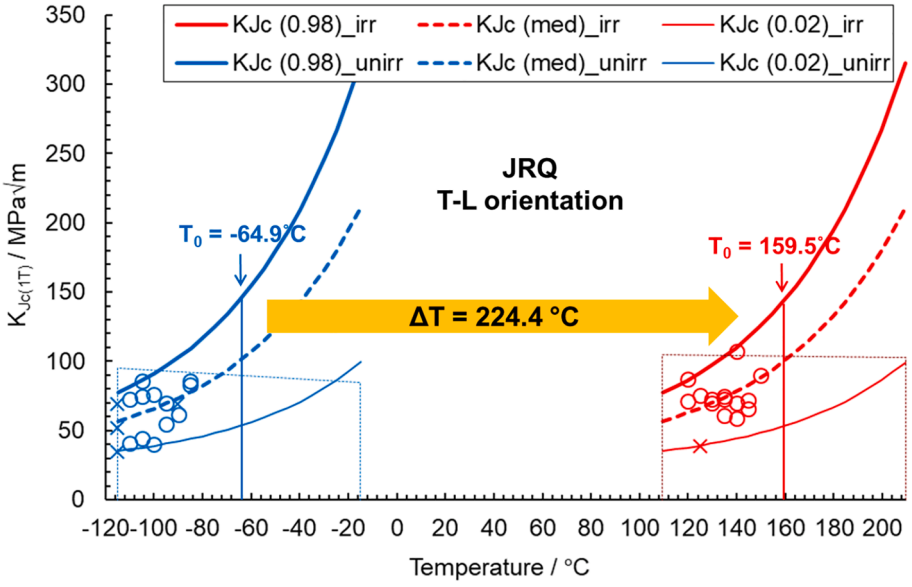

Fig. 2. $K_{Jc(1T)}$ versus temperature with K_{Jc} median (dashed) along with 98% and 2% tolerance bounds for JRQ T-L orientation in the unirradiated and the irradiated states showing the shift in reference temperature.

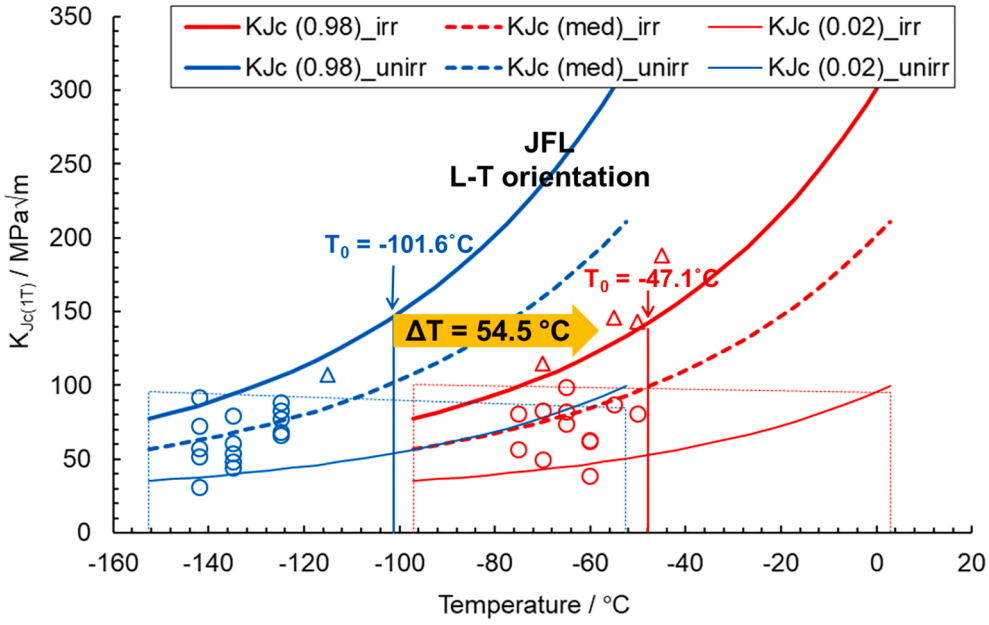

Fig. 3. $K_{Jc(1T)}$ versus temperature with K_{Jc} median (dashed) along with 98% and 2% tolerance bounds for JFL L-T orientation in the unirradiated and the irradiated states showing the shift in reference temperature.

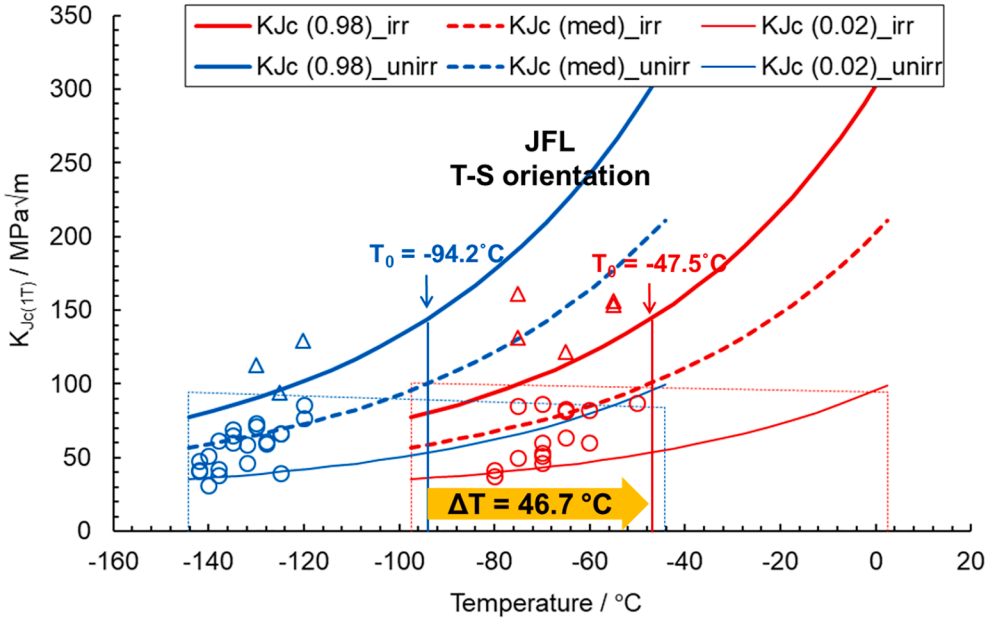

Fig. 4. $K_{Jc(1T)}$ versus temperature with K_{Jc} median (dashed) along with 98% and 2% tolerance bounds for JFL T-S orientation in the unirradiated and the irradiated states showing the shift in reference temperature.

Table 4
Master Curve results for JRQ and JFL in both unirradiated and irradiated states.

Material	Condition	Orientation	r	N	$\sum r_i \cdot n_i$	σ (K)	T_0 (°C)	ΔT_0 (K)
3JRQ57	Unirr	T-L	12	12	1.589	6.7	−64.9	–
		T-S	14	16	1.911	6.4	−67.8	–
	Irr	T-L	14	14	1.988	6.4	159.5	224.4
1JFL11	Unirr	L-T	15	16	2.054	6.3	−101.6	–
		T-S	22	25	2.875	5.9	−94.2	–
	Irr	L-T	12	16	1.833	6.7	−47.1	54.5
		T-S	15	20	2.214	6.3	−47.5	46.7

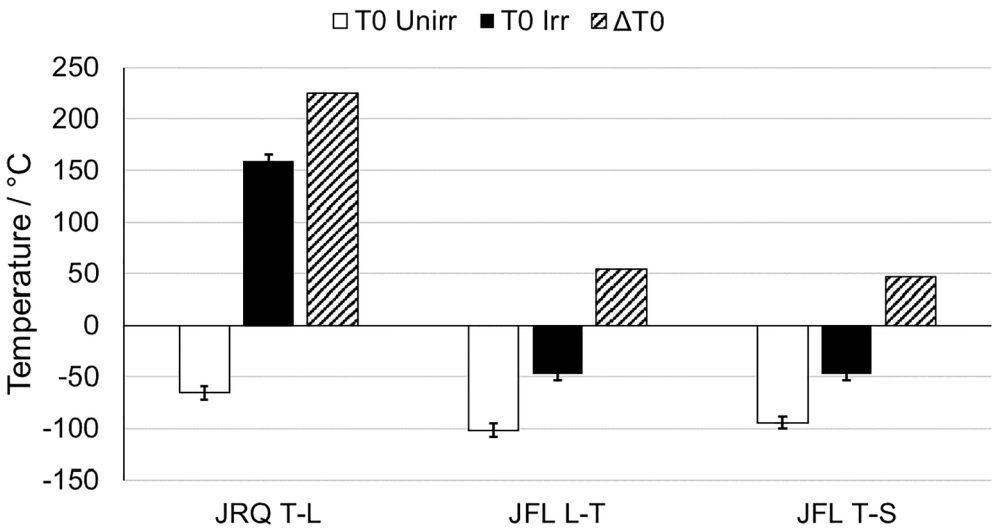

Fig. 5. The reference temperatures (T_0) for all the tested materials in both their unirradiated and irradiated states along with the shift in reference temperatures (ΔT_0).

Table 5
Reference temperatures of standard Charpy SE(B) and 0.16T C(T) specimens along with the standard deviations. The difference between the reference temperatures of standard Charpy-sized and 0.16T C(T) specimens is also listed (Δθ).

Material	Orientation	$T_0 \pm \sigma$ SE(B) (°C)	r SE(B)	N SE(B)	$\sum r_i \cdot n_i$ SE(B)	$T_0 \pm \sigma$ 0.16T C(T) (°C)	Δθ (K)
			Unirradiated				
3JRQ57	T-L	−65.6 ± 6.0	9	10	1.40	−64.9 ± 6.7	0.6
	T-S					−67.8 ± 6.4	2.3
1JFL11	L-T	−105.8 ± 4.7	16	18	2.38	−101.6 ± 6.3	4.2
	T-S					−94.2 ± 5.9	11.6
			Irradiated				
3JRQ57	T-L	164.2 ± 4.9	15	15	1.88	159.5 ± 6.4	4.7
	T-S						
1JFL11	L-T	−45 ± 3.8	22	23	3.35	−47.1 ± 6.7	2.1
	T-S					−47.5 ± 6.3	2.5

3.3. Censoring statistics

Based on 381 mini-C(T) tests from 11 different materials (Table 2), the absolute number of uncensored and censored tests at each temperature interval are shown in Fig. 8a. The number of tests performed for $T - T_0 < -10$ K were significantly higher than for $T - T_0 > -10$ K. Fig. 8b shows the relative probability of a test being censored at each temperature interval. The weighting factor n_i is highlighted for various temperature intervals as bars on top of Fig. 8b. The cumulative relative censoring probability is ≤15 % for $T - T_0 < -25$ K. The relative censoring frequency increases significantly for $T - T_0 > -10$ K.

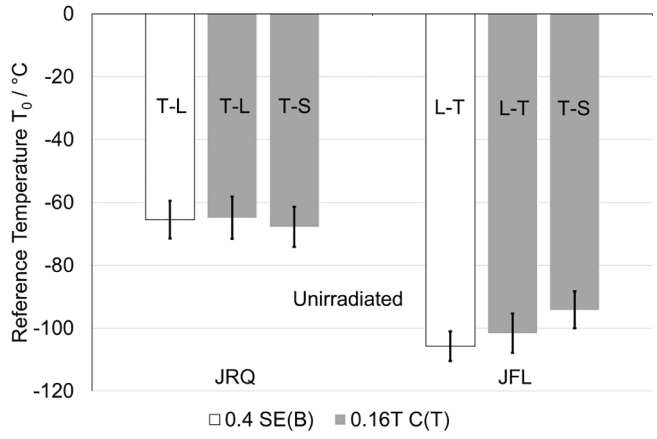

Fig. 6. Reference temperatures for unirradiated JRQ and JFL comparing the standard Charpy SE(B) and 0.16T C(T) specimens.

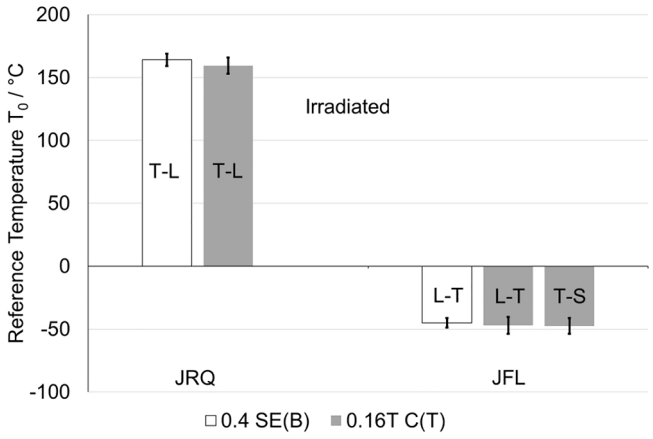

Fig. 7. Reference temperatures for irradiated JRQ and JFL comparing the standard Charpy SE(B) and 0.16T C(T) specimens.

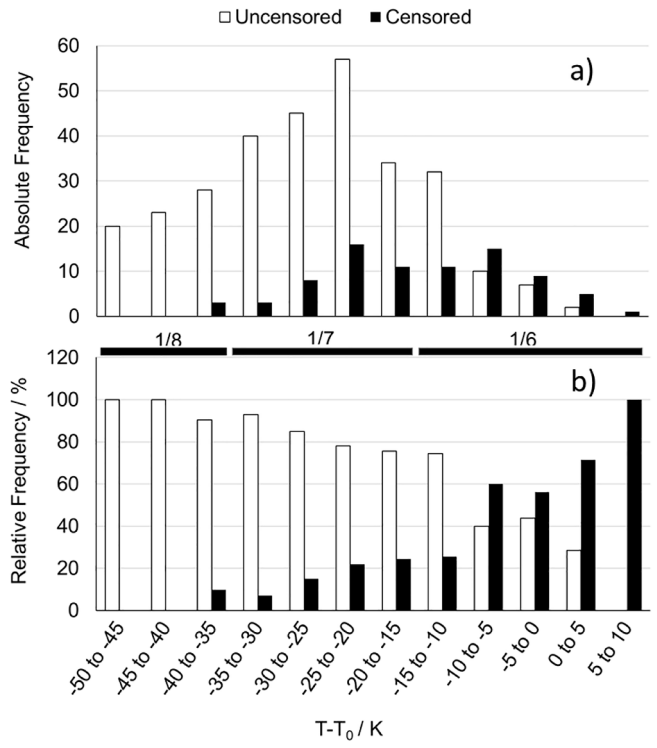

Fig. 8. Absolute a) and relative b) frequencies of uncensored and censored data in temperature intervals of 5 K ranging from −50 to 10 K. In b) the weighting factors (n) are shown for the different temperature ranges (bars on top).

3.4. The $K_{JcΔa}$ censoring criterion

For the verification of the $K_{JcΔa}$ censoring criterion, we selected 156 tests from the 381 tests listed in Table 2, 89 in the unirradiated and 67 in the irradiated state. The selection was performed taking into consideration that at least one test was violating the $K_{JcΔa}$ criterion in a test series (bold values in Table 6). Out of the 156 tests, the $K_{Jclimit}$ criterion is violated in 36 samples while the $K_{JcΔa}$ criterion is violated in 29 samples as shown in Table 6. The number of samples where both criteria are violated is 23. T_0 is calculated taking into account the violation of both the $K_{Jclimit}$ and the $K_{JcΔa}$ censoring criterion. It is also calculated for the case when the $K_{JcΔa}$ censoring criterion is not considered (only the $K_{Jclimit}$ criterion is considered). The ΔT_k (difference between T_0 calculated with and without $K_{JcΔa}$ censoring criterion) and σ (standard deviation with the $K_{JcΔa}$ censoring criterion) for different materials are listed in Table 6 as well as highlighted in Fig. 9. The average ΔT_k for these samples was 2.8 °C, a value lower than the average standard deviation of 7.2 °C for these samples (Table 6).

4. Discussion

4.1. The effect of initial microstructure and neutron irradiation on Master Curve

The reference temperature of unirradiated JRQ comes out to be very close to the T_0 value reported in [12]. Only a small variation in T_0, falling within the bounds of the standard deviation, was observed for tests in different orientations. This is due to the microstructure of the materials which went through the austenization process resulting in equiaxed grains [38], and any texture is weakened by the bainitic transformation. A detailed microstructural analysis of JRQ and JFL will be performed in another study.

The shift in reference temperature from unirradiated to the irradiated state is the highest for the JRQ material due to the higher amounts of Cu and P in its composition that results in the formation of Cu-rich and phosphide precipitates. This has been also observed in various other studies [21–24].

4.2. Comparison of standard Charpy-sized and mini-C(T) specimen

The difference between the T_0 of standard Charpy-sized and mini-C(T) specimen (Δθ) in the T-L orientation came out to be 0.6 K for JRQ unirradiated specimen (Table 5) which is similar to the difference reported by [12]. The difference between standard Charpy-sized and the mini-C(T) specimen tested in the unirradiated T-S orientation (2.3 K)

Table 6
List of specimens analysed with the $K_{Jclimit}$ and $K_{JcΔa}$ censoring criterion along with the T_0 calculated with and without the $K_{JcΔa}$ censoring criterion. The difference between T_0 calculated with and without $K_{JcΔa}$ censoring criterion (ΔT_k) as well as the standard deviation (σ) is also listed. Values in bold represent the specimens selected to verify the $K_{JcΔa}$ censoring criterion. ***Total and average are calculated from the bold values.**

Material	Condition	Orientation	Testing temperature range $T - T_0$ (K)	r	N	$K_{Jclimit}$ violation	$K_{JcΔa}$ violation	T_0 with $K_{JcΔa}$ (°C)	$T_0^{'}$ without $K_{JcΔa}$ (°C)	ΔT_k (K)	σ (K)
3JRQ57	Unirr	T-L	−50.1 to −20.1	12	12	0	0	−64.9	−64.9	0	6.7
		T-S	**−47.2 to −22.2**	**14**	**16**	**2**	**1**	**−67.8**	**−69.5**	**1.7**	**6.4**
	Irr	T-L	−39.5 to 9.5	14	14	0	0	159.5	159.5	0	6.4
1JFL11	Unirr	L-T	−40.4 to −13.4	15	16	1	0	−101.6	−101.6	0	6.3
		T-S	−47.8 to −25.8	22	25	3	0	−94.2	−94.2	0	5.9
	Irr	**L-T**	**−27.9 to 2.1**	**12**	**16**	**4**	**3**	**−47.1**	**−47.3**	**0.2**	**6.7**
		T-S	**−32.5 to −2.5**	**15**	**20**	**5**	**3**	**−47.5**	**−50.9**	**3.4**	**6.3**
ANP-6	Unirr	**T-L**	**−25.3 to −5.3**	**7**	**11**	**4**	**1**	**−84.7**	**−85.5**	**0.8**	**8.2**
		T-S	**−29 to 6**	**9**	**12**	**3**	**3**	**−106**	**−107.4**	**1.4**	**7.4**
		S-L	−46.8 to −26.8	8	8	0	0	−73.2	−73.2	0	8.2
	Irr	**T-S**	**−21.5 to 8.5**	**9**	**15**	**2**	**6**	**101.5**	**106.2**	**4.7**	**7.2**
ANP-3	Unirr	**T-L**	**−36.2 to −11.2**	**11**	**16**	**4**	**5**	**−98.8**	**−100**	**1.2**	**6.9**
	Irr	**T-L**	**−26.2 to −6.2**	**11**	**16**	**5**	**1**	**−38.8**	**−39.7**	**0.9**	**6.9**
ANP-2	Unirr	S-L	−25.1 to 24.9	7	12	5	0	−54.9	−54.9	0	7.9
		T-S	−25.6 to −15.6	5	6	1	0	−54.4	−54.4	0	9.3
ANP-5	Unirr	**S-L**	**−48 to −28**	**9**	**10**	**1**	**1**	**−22**	**−28.7**	**6.7**	**7.8**
		T-L	−45.9 to −25.9	9	9	0	0	−24.1	−24.1	0	7.8
		T-S	**−43.6 to −23.6**	**9**	**12**	**2**	**3**	**−26.4**	**−33.9**	**7.5**	**7.8**
FZD-4	Unirr	**L-S**	**−28.1 to −8.1**	**8**	**12**	**4**	**2**	**−101.9**	**−104.1**	**2.2**	**7.8**
		L-T	−24.9 to −4.9	10	12	2	0	−115.1	−115.1	0	7.2
		S-T	−42.8 to −22.8	9	10	1	0	−97.2	−97.2	0	7.4
CRIEPI	Unirr	T-S	−30.7 to −10.7	17	22	5	0	−102	−102	0	6.1
	Total*			**114**	**156**	**36**	**29**		**Average***	**2.8**	**7.2**

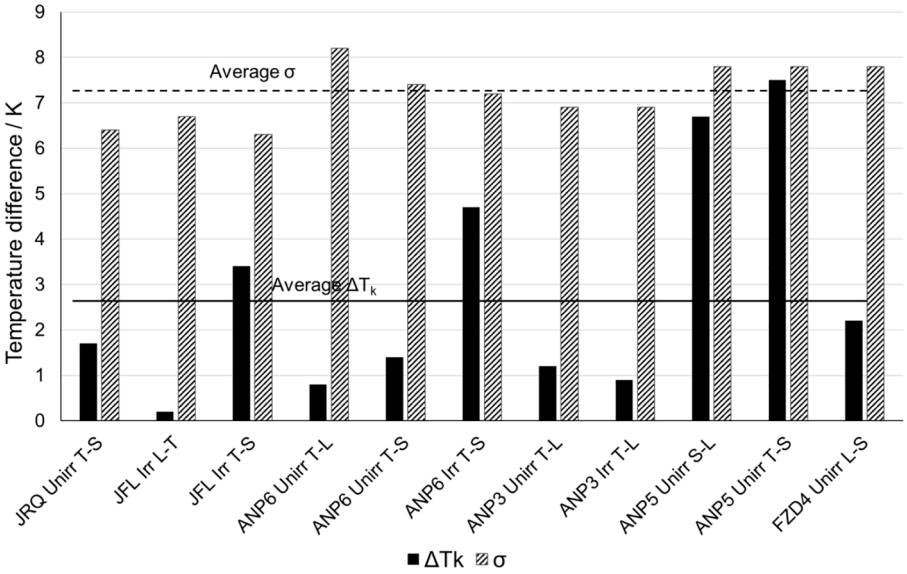

Fig. 9. The ΔT_k and σ values from Table 6 for various materials. The dashed line indicates the average standard deviation while the solid line indicates the average temperature difference.

was also within the standard deviations of both SE(B) (6.0 K) and mini-C(T) specimen testing (6.4 K). A T_0 higher by ≈ 10 K was reported in [13] for JRQ using mini-C(T) as compared to standard Charpy-sized specimens. For JFL, a T_0 higher by 4.2 K and 11.6 K was obtained for the L-T and T-S oriented mini-C(T), respectively as compared to the L-T oriented standard Charpy-sized specimen. While the Δθ for the L-T orientation (4.2 K) is within the bounds of the standard deviation of the mini-C(T) test series (6.3 K), the Δθ for the T-S orientation (11.6 K) is close to the cumulative standard deviations of the mini-C(T) and standard Charpy-sized specimen tests (4.7 + 5.9 = 10.6 K). Miura and Soneda reported similar T_0 for mini-C(T) and standard Charpy-sized specimens for JFL [13].

Similar comparative results were also observed for the irradiated specimens in all the orientations for JRQ and JFL where a slightly lower T_0 was obtained for mini-C(T) as compared to standard Charpy-sized specimens (Table 5) thus demonstrating the validity of the application of mini-C(T) specimens. A slightly lower T_0 for irradiated mini-C(T) specimen was also obtained in [12] where the neutron fluence was an order of magnitude lower compared to the present study.

4.3. Statistically based concept for optimum test temperature selection

In the current version of ASTM E1921 (section 10.3), the selection of test temperatures is discussed on a non-quantitative basis. Moreover, the suggestions do not consider the censoring behavior of mini-C(T) specimens (which is different from standard Charpy-sized specimens). This may lead to an unnecessarily high number of tests required for a valid T_0-evaluation. The proposed procedure aims at optimizing the use of available mini-C(T) samples. Based on the censoring statistics presented in section 3.3, the probability, that a test datum at a certain temperature will be censored (i.e., $K_{Jc} > K_{Jclimit}$ or $K_{Jc} > K_{JcΔa}$), can empirically be approximated by a tanh-fit as follows:

$$P_c = 0.5 + 0.5 \cdot \tanh[c \cdot (T - T_0 + T_{sh})] \quad (1)$$

The tanh-fit is shown in Fig. 10. The relative frequencies from Fig. 8b were used. The obtained fitting parameters are $c = 0.056$ and $T_{sh} = 7.9$K, using the complete data set of 381 tests.

By means of this analytical description of the censoring probability, a statistically based strategy for the selection of test temperatures can be established. The temperatures of the first 3–5 tests have to be selected on the basis of the expected reference temperature. The temperature interval $T_{0,exp} - 30K < T < T_{0,exp} - 25K$ is a reasonable choice. Based on these first few data points, a preliminary T_0 can be calculated. The selection of the temperature of the next test is based on a target censoring probability:

$$T = T_0 - T_{sh} + \frac{1}{c} \cdot \arctan\left[\frac{P_{c,trg} - 0.5}{0.5}\right] \quad (2)$$

which corresponds to equation (1) rearranged for solving T. The target censoring probability $P_{c,trg}$ is chosen in dependence of two parameters, $s_{rn} = \sum r_i n_i$ and r/N, calculated from the currently available test data (where r is the number of uncensored valid data and N is the total number of valid data; as for s_{rn}, r_i and n_i cf. ASTM E1921, section 10.3) [27]. The following approach is used:

$$P_{c,trg} = 0.05 + 0.9 \cdot \left[\min\left(\frac{s_{rn}}{3}, 1\right)\right]^p \cdot \left[\frac{r}{N}\right]^q \quad (3)$$

i.e., $0.05 \le P_{c,trg} \le 0.95$. The parameters are $p = 0.7$ and $q = 1.1$, which ensures that the following condition is fulfilled:

$$P_{c,trg} < 0.5 \quad \forall \quad s_{rn} < 1 \text{ and } r/N < 0.5 \quad (4)$$

The target censoring probability is shown in Fig. 11. The procedure

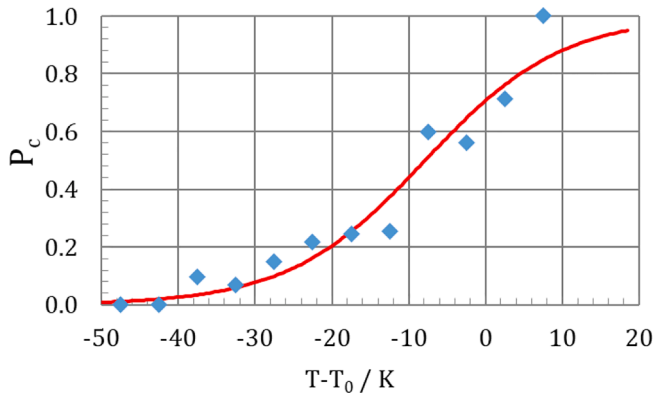

Fig. 10. Tanh-fit of the censoring probability plotted against $T - T_0$

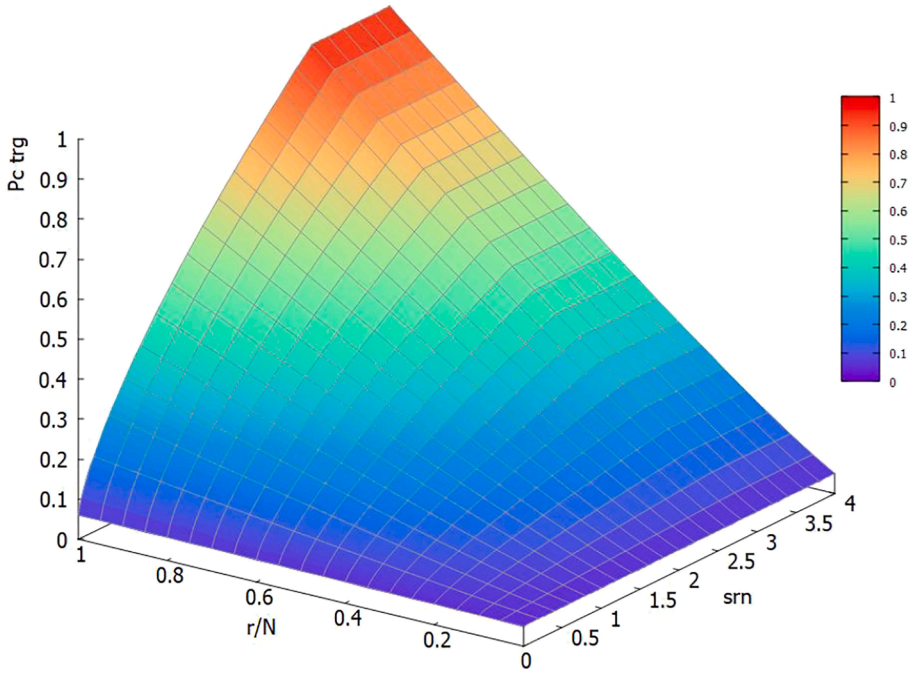

Fig. 11. Target censoring probability as function of s_{rn} and r/N.

based on equations (2) to (4) is repeated after each new test. This concept quantifies the balance between the two competing aspects of temperature selection: testing close to T_0 and avoidance of censoring (cf. introduction).

4.4. The impact of $K_{JcΔa}$ censoring criterion on T_0

At testing temperatures close to T_0, the $K_{Jclimit}$ and the $K_{JcΔa}$ censoring criteria both tend to be violated. As seen from the results in Table 6, there are 23 samples where both the criteria are simultaneously violated. The inclusion of $K_{JcΔa}$ censoring criterion results in a small increase in T_0 as compared to the case when only the $K_{Jclimit}$ censoring criterion is considered. Since this increase (ΔT_k) falls below the standard deviation of individual Master Curve tests (Fig. 10), it is reasonable to say that the impact of the slow stable crack growth censoring criterion on T_0 is insignificant. Therefore, to make the determination of T_0 simpler and to avoid additional time-consuming analysis of the fracture surface, the $K_{JcΔa}$ censoring criterion could be removed.

5. Conclusion

This work validates the use of mini-C(T) specimens for JRQ and JFL in their unirradiated and irradiated conditions for Master Curve testing and confirms the detrimental effects of impurity elements like Cu and P. It additionally suggests improvements for the optimization of the Master Curve testing and analysis. Our findings are summarized as follows:

- JRQ exhibits a higher shift in T_0 due to the presence of impurity elements such as Cu and P. The testing orientation of the samples did not significantly influence the T_0.
- The T_0 obtained from mini-C(T) specimens agrees with the T_0 obtained from standard Charpy-sized specimens confirming the successful use of mini-C(T) specimens.
- We established an empirical correlation between test temperature and censoring probability using censoring statistics from a large number of mini-C(T) test data. Based on this, we propose a concept for the optimum choice of test temperature within a Master Curve analysis.
- The $K_{JcΔa}$ censoring criterion does not influence the T_0 significantly. Hence, we suggest a simplification of ASTM E1921 for the Master Curve analysis.

Future work on connecting the bulk microstructures to the fracture properties through advanced microscopy techniques is in progress.

CRediT authorship contribution statement

A. Das: Conceptualization, Validation, Investigation, Writing – original draft, Writing – review & editing. **P. Chekhonin:** Validation, Writing – review & editing. **M. Houska:** Methodology, Investigation, Resources. **F. Obermeier:** Validation, Writing – review & editing. **E. Altstadt:** Conceptualization, Methodology, Software, Validation, Formal analysis, Writing – review & editing, Supervision, Funding acquisition.

Declaration of Competing Interest

The authors declare that they have no known competing financial interests or personal relationships that could have appeared to influence the work reported in this paper.

Data availability

Data will be made available on request.

Acknowledgements

We acknowledge the financial support of this research by the German BMWi project “Kleinproben” (FKZ 1501598A/B) and by the EU-Euratom project “Fractesus” (contract no. 900014). The authors express their gratitude to W. Webersinke, M. Roßner, V. Reinke, J. Pietzsch and T. Welz for their valuable technical support.

References

[1] K. Wallin, The scatter in KIC-results, Eng. Fract. Mech. 19 (1984) 1085–1093, https://doi.org/10.1016/0013-7944(84)90153-X.

[2] K. Wallin, The size effect in KIC results, Eng. Fract. Mech. 22 (1985) 149–163, https://doi.org/10.1016/0013-7944(85)90167-5.
[3] K. Wallin, Irradiation damage effects on the fracture toughness transition curve shape for reactor pressure vessel steels, Int. J. Press. Vessels Pip. 55 (1993) 61–79, https://doi.org/10.1016/0308-0161(93)90047-W.
[4] A. Ballesteros, E. Altstadt, F. Gillemot, H. Hein, J. Wagemans, J. Rouden, J. Barthelmes, K. Wilford, M. Serrano, M. Brumovsky, R. Chaouadi, S. Ortner, Monitoring radiation embrittlement during life extension periods, Nucl. Eng. Des. 267 (2014) 197–206, https://doi.org/10.1016/j.nucengdes.2013.11.068.
[5] C. Zurbuchen, H.-W. Viehrig, F.-P. Weiss, Master Curve and Unified Curve applicability to highly neutron irradiated Western type reactor pressure vessel steels, Nucl. Eng. Des. 239 (2009) 1246–1253, https://doi.org/10.1016/j.nucengdes.2009.03.008.
[6] R. Chaouadi, M. Scibetta, E. Van Walle, R. Gerard, On the Use of the Master Curve based on the Precracked Charpy Specimen, ASME Press. Vessel Pip. Symp. 393 (1999) 35–46.
[7] R.K. Nanstad, D.E. McCabe, M.A. Sokolov, J.G. Merkle, Experimental Evaluation of Deformation and Constraint Characteristics in Precracked Charpy and Other Three-Point Bend Specimens, in: American Society of Mechanical Engineers Digital Collection, 2009, pp. 259–267. https://doi.org/10.1115/PVP2007-26651.
[8] H.-W. Viehrig, M. Scibetta, K. Wallin, Application of advanced master curve approaches on WWER-440 reactor pressure vessel steels, Int. J. Press. Vessels Pip. 83 (2006) 584–592, https://doi.org/10.1016/j.ijpvp.2006.04.005.
[9] R. Chaouadi, E. van Walle, M. Scibetta, R. Gérard, On the Use of Miniaturized CT Specimens for Fracture Toughness Characterization of RPV Materials, in: American Society of Mechanical Engineers Digital Collection, 2016. https://doi.org/10.1115/PVP2016-63607.
[10] E. van Walle, M. Scibetta, M.J. Valo, H.-W. Viehrig, H. Richter, T. Atkins, M. R. Wootton, E. Keim, L. Debarberis, M. Horsten, Reconstitution techniques qualification and evaluation to study ageing phenomena of nuclear pressure vessel materials (RESQUE), Nucl. Eng. Des. 209 (2001) 67–77, https://doi.org/10.1016/S0029-5493(01)00389-2.
[11] M. Scibetta, E. Lucon, R. Chaouadi, E. van Walle, R. Gérard, Use of Broken Charpy V-notch Specimens from a Surveillance Program for Fracture Toughness Determination, J. ASTM Int. 3 (2005) 1–7, https://doi.org/10.1520/JAI12450.
[12] M. Yamamoto, The Master Curve Fracture Toughness Evaluation of Irradiated Plate Material JRQ Using Miniature-C(T) Specimens, in: PVP2017, Volume 1A: Codes and Standards, 2017. https://doi.org/10.1115/PVP2017-66085.
[13] N. Miura, N. Soneda, Evaluation of Fracture Toughness by Master Curve Approach Using Miniature C(T) Specimens, J. Press. Vessel Technol. 134 (2012), https://doi.org/10.1115/1.4005390.
[14] M. Yamamoto, Trial Study of the Master Curve Fracture Toughness Evaluation by Mini-C(T) Specimens for Low Upper Shelf Weld Metal Linde-80, in: American Society of Mechanical Engineers Digital Collection, 2018. https://doi.org/10.1115/PVP2018-84906.
[15] M.A. Sokolov, Use of Mini-CT Specimens for Fracture Toughness Characterization of Low Upper-Shelf Linde 80 Weld Before and After Irradiation, in: American Society of Mechanical Engineers Digital Collection, 2018. https://doi.org/10.1115/PVP2018-84804.
[16] M. Yamamoto, R. Carter, H.-W. Viehrig, M. Lambrecht, A Round Robin Program of MasterCurve Evaluation Using Miniature C(T) Specimens (Comparison of T0 for a Weld Metal), in: IASMiRT, BEXCO, Busan, Korea, 2017, p. 10.
[17] M. Yamamoto, A. Kimura, K. Onizawa, K. Yoshimoto, T. Ogawa, Y. Mabuchi, H.-W. Viehrig, N. Miura, N. Soneda, A Round Robin Program of Master Curve Evaluation Using Miniature C(T) Specimens: 3rd Report — Comparison of T0 Under Various Selections of Temperature Conditions, in: American Society of Mechanical Engineers Digital Collection, 2014. https://doi.org/10.1115/PVP2014-28898.
[18] K. Wallin, M. Yamamoto, U. Ehrnstén, Location of Initiation Sites in Fracture Toughness Testing Specimens: The Effect of Size and Side Grooves, in: PVP2016, Volume 1B: Codes and Standards, 2016. https://doi.org/10.1115/PVP2016-63078.
[19] M. Yamamoto, N. Miura, Applicability of Miniature C(T) Specimens for the Master Curve Evaluation of RPV Weld Metal, in: PVP2015, Volume 1A: Codes and Standards, 2015. https://doi.org/10.1115/PVP2015-45545.
[20] T. Sugihara, T. Hirota, H. Sakamoto, K. Yoshimoto, K. Tsutsumi, T. Murakami, Applicability of Miniature C(T) Specimen to Fracture Toughness Evaluation for the Irradiated Japanese Reactor Pressure Vessel Steel, in: American Society of Mechanical Engineers Digital Collection, 2017. https://doi.org/10.1115/PVP2017-66206.
[21] G.R. Odette, G.E. Lucas, Recent progress in understanding reactor pressure vessel steel embrittlement, Radiat. Eff. Defects Solids 144 (1998) 189–231, https://doi.org/10.1080/10420159808229676.
[22] M.K. Miller, R.K. Nanstad, M.A. Sokolov, K.F. Russell, The effects of irradiation, annealing and reirradiation on RPV steels, J. Nucl. Mater. 351 (2006) 216–222, https://doi.org/10.1016/j.jnucmat.2006.02.010.
[23] E. Altstadt, E. Keim, H. Hein, M. Serrano, F. Bergner, H.-W. Viehrig, A. Ballesteros, R. Chaouadi, K. Wilford, FP7 Project LONGLIFE: Overview of results and implications, Nucl. Eng. Des. 278 (2014) 753–757, https://doi.org/10.1016/j.nucengdes.2014.09.003.
[24] H.-W. Viehrig, E. Altstadt, M. Houska, M. Valo, Fracture mechanics characterisation of the beltline welding seam of the decommissioned WWER-440 reactor pressure vessel of nuclear power plant Greifswald Unit 4, Int. J. Press. Vessels Pip. 89 (2012) 129–136, https://doi.org/10.1016/j.ijpvp.2011.10.016.
[25] INTERNATIONAL ATOMIC ENERGY AGENCY, Reference Manual on the IAEA JRQ Correlation Monitor Steel for Irradiation Damage Studies, IAEA. Report number IAEA-TECDOC-1230, 2001.
[26] H.-W. Viehrig, C. Zurbuchen, Application of the Master Curve regarding characterization of the toughness of neutron irradiated Reactor Pressure Vessel steels, HZDR. Internal report FZD-476 2007, 2007.
[27] E08 Committee, Test Method for Determination of Reference Temperature, To, for Ferritic Steels in the Transition Range ASTM E1921-2021, ASTM International, n.d. https://doi.org/10.1520/E1921-21.
[28] M. Brumovsky, L. Davies, A. Kryukov, V. Lyssakov, R. Nanstad, Reference manual on the IAEA JRQ correlation monitor steel for irradiation damage studies, Int. At. Energy Agency Vienna Austria Rep. No IAEA-TECDOC-1230. (2001). http://www-pub. iaea. org/MTCD/Publications/PDF/te_1230_prn. pdf.
[29] A. Ulbricht, H. Hein, M. Hernandez-Mayoral, E. Onorbe, A. Etienne, E. Meslin, M. Brumovsky, The effect of neutron flux on irradiation induced damage of RPV steels, SOTERIA. Report D2.1, 2018.
[30] S. Ritter, H.P. Seifert, Characterisation of the Lower Shell and Weld Material of the Biblis C Reactor Pressure Vessel, Paul Scherrer Institut, CH – 5232 Villigen PSI, 2002.
[31] M. Serrano, J. Lydman, C. Hurley, W. Karlsen, J. Kobiela, H. Hein, M. Neukam, B. Radiguet, F. Bergner, H.-W. Viehrig, R. Hernandez, Microstructural Inhomogeneities of RPV Steels and Their Impact On Mechanical Properties at Initial State, SOTERIA. Report D3.1, 2017.
[32] H.-W. Viehrig, A. Ulbricht, F. Bergner, H. Hein, B. Radiguet, J. Lydman, W. Karlsen, M. Brumovsky, M. Hernandez-Mayoral, Effects of initial materials inhomogeneities on microstructure and mechanical properties of RPV steels at irradiated state for LTO, SOTERIA. Report D3.2, 2019.
[33] M. Scibetta, E. Lucon, E. van Walle, Optimum use of broken Charpy specimens from surveillance programs for the application of the master curve approach, Int. J. Fract. 116 (2002) 231–244, https://doi.org/10.1023/A:1020165900918.
[34] E. Altstadt, F. Bergner, M. Houska, Use of the small punch test for the estimation of ductile-to-brittle transition temperature shift of irradiated steels, Nucl. Mater. Energy. 26 (2021), 100918, https://doi.org/10.1016/j.nme.2021.100918.
[35] H. Hein, J. Barthelmes, F. Gillemot, M. Serrano, Hernandez-Mayoral, Documentation and data of materials for microstrucural analysis, LONGLIFE. Report D3.1 revision 2, 2012.
[36] Reaktorsicherheitskommission, RSK-guidelines for PWR reactors, RSK-Leitlinien Fuer Druckwasserreaktoren, 1979.
[37] J.D. Landes, J calculation - front face displacement measurement on a compact specimen, Int. J. Fract. 16 (1980).
[38] M. Yamamoto, S. Ukai, S. Hayashi, T. Kaito, S. Ohtsuka, Reverse phase transformation from α to γ in 9Cr-ODS ferritic steels, J. Nucl. Mater. 417 (2011) 237–240, https://doi.org/10.1016/j.jnucmat.2010.12.250.